Hydrogel Pore-Size Modulation for Enhanced Single-Cell Western Blotting

*Todd A. Duncombe, Chi-Chih Kang, Santanu Maity, Toby M. Ward, Mark D. Pegram, Niren Murthy, and Amy E. Herr**

Dysregulation of signaling pathways, and cell-to-cell variation of the same, is a hallmark of cancer.[1] While single-cell resolution genomic and transcriptomic tools are advancing, these nucleic acid measurements do not directly measure protein-mediated signaling including dynamic post-translational protein modifications, protein localization, and protein–protein interactions. A majority of cancer therapies target proteins and tumoral heterogeneity drives both drug response and resistance.[2,3] Single-cell resolution proteomic tools can provide new insights.

Advanced single-cell protein analysis tools do exist, yet all contemporary approaches to detect endogenous proteins are immunoassays (e.g., immunohistochemistry/immunocytochemistry (IHC/ICC),[4] flow,[5] mass cytometry,[6] and various enzyme-linked immunosorbent assays including microfluidic formats).[7] While powerful, the analytical specificity of immunoassays is dictated by immunoreagents (e.g., antibodies). Suboptimal performance and unavailable immunoreagents severely curtail multiplexing capacity (e.g., off-target background signal) and the range of protein targets (especially isoforms).[8,9] To mitigate off-target immunoreagent binding, researchers prepend an electrophoretic protein separation to the immunoassay, thereby loosening constraints on immunoreagent performance and enhancing assay specificity. This combined protein separation and immunoassay is known as a western blot.[10–12] Unfortunately, the conventional western blot requires pooling of thousands of cells for each measurement, thus obscuring important cell-to-cell variation in protein expression and state.

We recently developed a photoactive hydrogel to achieve single-cell resolution western blotting.[13,14] Central to the single-cell separations capability is a multifunctional hydrogel, common in drug delivery[15,16] and tissue engineering,[17–19] yet not as often applied in separation science. Exposure of the hydrogel to UV light activates benzophenone methacrylamide cross-linked into the gel to covalently immobilize electrophoretically resolved proteins onto the gel.[12] Thus, the polyacrylamide gel (PAG) toggles from a molecular sieving matrix (for protein electrophoresis) to a protein immobilization scaffold (for in-gel immunoprobing). Soft lithography allows us to cast thousands of microwells in this photofunctional hydrogel layered on a silanized microscope slide. Microwells both isolate individual cells and seamlessly integrate in-well cell lysis with subsequent single-cell western blotting. While throughput is exceptional (>6000 concurrent single-cell protein assays),[13,14] the hydrogel cannot resolve the broad molecular mass range of proteins involved in signaling networks. Single-cell polyacrylamide gel electrophoresis (PAGE) over such short distances can only resolve molecular mass differences exceeding 50%.[13]

Two material advances are introduced here to progress single-cell protein separation science. First, a spatially modulated (i.e., large-to-small) pore-size gradient sieving matrix is needed to electrophoretically resolve protein pairs spanning a broad molecular mass range.[20] Yet, conventional fabrication approaches cannot form thousands of ≈1 mm long pore-size gradient gels on a microscope slide, with each lane precisely aligned with a 30 µm diameter microwell.[21,22] Here, we introduce a fabrication approach which combines grayscale photolithography and a glass-SU8 mold to pattern gel density with high spatial resolution. In one UV exposure step, we create 3402 microscale pore-gradient electrophoresis gels packed into the footprint of a standard glass microscope slide (**Figure 1**a), each pore-gradient aligned with a molded microwell for single-cell isolation. The pore-gradient gel array achieves optimal single-cell protein separation in 1 mm long separation lanes and is suitable for proteins spanning an order of magnitude in molecular mass (Figure 1b,c). The pore-gradient PAG fabrication and single-cell protein PAGE procedure are detailed in the Supporting Information. The composition of all PAG is detailed in Table S1 (Supporting Information).

Second, a temporally modulated PAG cross-linker density is needed to ensure uniform introduction of antibody probes into the pore-gradient gels after the separation is performed. We hypothesize that nonuniform pore-size gels will result in nonuniform local immunoreagent concentrations, thus spatially biasing immunoassay performance depending on molecular mass of the target being probed. To overcome this nonuniform partitioning of immunoreagents, we develop a dual cross-linked PAG formulation containing both methylene bisacrylamide (BIS) and *N,N′*-[(1-methylethylidene)bis(oxy-2,1-ethanediyl)] diacrylamide (diacrylamide ketal, DK). After protein PAGE and

Dr. T. A. Duncombe, Dr. C.-C. Kang,
Dr. S. Maity, Prof. N. Murthy, Prof. A. E. Herr
Department of Bioengineering
University of California Berkeley
Berkeley, CA 94720, USA
E-mail: aeh@berkeley.edu

Dr. T. A. Duncombe, Prof. N. Murthy, Prof. A. E. Herr
The UC Berkeley/UCSF Graduate Program in Bioengineering
University of California Berkeley
Berkeley, CA 94720, USA

Dr. T. M. Ward, Prof. M. D. Pegram
Division of Oncology
Department of Medicine
Stanford University
Stanford, CA 94305, USA

DOI: 10.1002/adma.201503939

ADVANCED MATERIALS
www.advmat.de

www.MaterialsViews.com

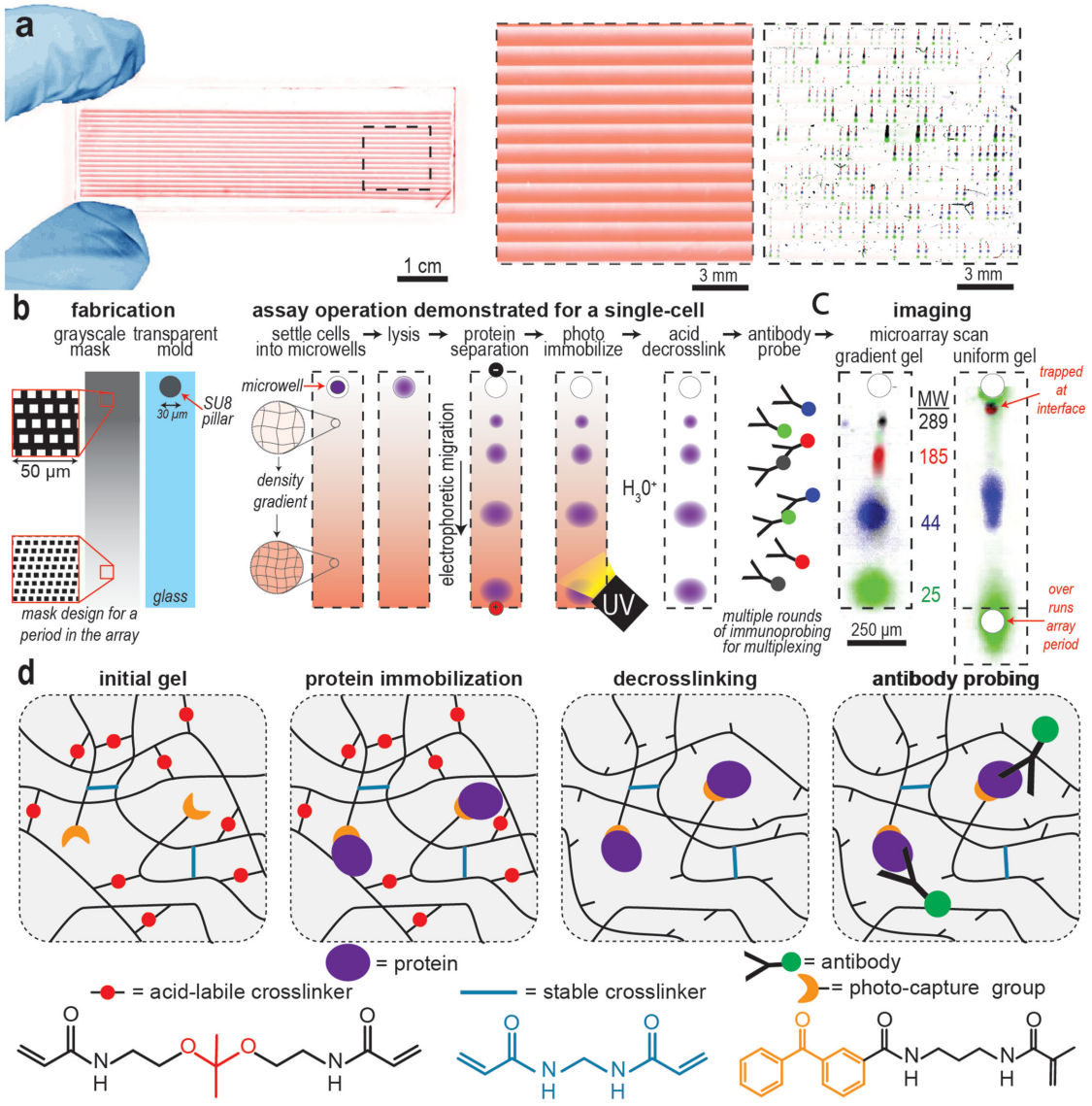

Figure 1. Multifunctional hydrogel enables western blotting of wide mass range proteins across thousands of individual cells on a microscope slide. a) A false-color image of an entire array of pore-gradient gels patterned on a microscope slide, each supports polyacrylamide gel electrophoresis (PAGE) of a single-cell lysate. The pore-gradient of the gel is revealed by incorporating FITC and visualized with fluorescence imaging. Close-up false color fluorescence micrograph shows one block of over 400 pore-gradient PAGE lanes (middle). Microwells isolate individual cells for achieving western blotting at single-cell resolution (right). b) Grayscale photolithography used in conjunction with a transparent glass-SU8 mold creates an array of microwells aligned to 1 mm long pore-gradient gels. The grayscale mask design for one period of the gradient-array is displayed. The grayscale mask attenuates UV dose during gel photopolymerization yielding spatially varying polymerization kinetics and, thus, spatially varying gel density (left). After single cells are passively settled into each microwell through a gravity-driven process[13] (Figure S2, Supporting Information) and in situ chemical lysis in a microwell, single-cell western blotting is performed. During single-cell lysate PAGE, the large-to-small pore-gradient gel is useful for resolving wide molecular mass range proteins. The gel contains benzophenone methacrylamide such that brief UV exposure covalently immobilizes separated proteins to the hydrogel during blotting. After blotting, the gel is soaked in HCl to cleave the DK cross-linkers, thus expanding the pores to enhance the local in-gel antibody concentration for immunoprobing, while BIS cross-linkers maintain mechanical integrity. c) Fluorescence images of single-cell western blots for HER2 signaling proteins spanning 25–289 kDa. Pore-gradient PAGE requires <1 mm separation length to resolve the species (left), whereas a uniform pore-size gel cannot resolve both high and low molecular mass protein pairs (right). d) Schematic of gel pore expansion by acid hydrolysis for uniform in-gel immunoprobing in dual-cross-linked gels. The acid-labile cross-linker is *N,N′*-[(1-methylethylidene)bis(oxy-2,1-ethanediyl)]diacrylamide (diacrylamide ketal, DK). The stable cross-linker is methylene bisacrylamide (BIS). The photocapture group is *N*-[3-[(3-benzoylphenyl)formamido]propyl] methacrylamide (BPMAC).

photoinduced protein immobilization, acid hydrolysis cleaves the ketal group on the DK to break the cross-linker and expand the hydrogel pores, introducing efficient and spatially unbiased in-gel immunoprobing after protein immobilization (Figure 1d). Accordingly, through incorporation of a spatially–temporally modulated multifunctional hydrogel, we aim to bring high-resolution western blotting to single breast cancer cells (Figure 1a, right panel).

Adv. Mater. **2015**,
DOI: 10.1002/adma.201503939

In the gradient microgel prong of our study, we sought to create thousands of micron-scale pore-gradient gels using a grayscale photomask. A grayscale photomask spatially attenuates UV intensity,[23] thus locally altering the rate of free-radical production and polymerization.[24] If polymerization is halted prior to completion, the grayscale mask opacity determines the local effective gel density. Others have used PAG grayscale photopatterning to create cellular niches with a variety of mechanical stiffness.[25] To create pore-gradient microgels, we employ a chrome grayscale photomask (≈3–10 µm chrome dots; Figures S1 and S3, Supporting Information) and expose to UV light through a 390 nm long-pass filter to activate the azo-initiator in our gel precursor solution. The long-pass filter is critical in photopolymerization to prevent the activation of gel-incorporated benzophenone, such that the benzophenone is available for subsequent protein capture (blotting) after electrophoresis.

To visualize the resultant pore-gradient microgels, we incorporated allylamine in the gel precursor solution (1:100 molar ratio with acrylamide), then labeled the primary amine with fluorescein isothiocyanate (FITC) and inferred acrylamide density using fluorescence imaging (**Figure 2**a,b and Figure S4, Supporting Information).[26] Optical profilometry of dehydrated pore-gradient gels revealed a gel height increase of 3.5 µm over each 1 mm separation distance (Figure 2a). While pore-gradient gels are relevant to single-cell PAGE of proteins spanning a large molecular mass range, a variety of pore-size distributions are possible. For example, periodic nonlinear pore-size gradients, step function stacking gels, and combinations of gel pore-size distributions are readily realized using this grayscale photopatterning approach (Figure 2b).

Next, to assess molecular sieving in the 1 mm long pore-gradient microgels, we assayed a model GFP-transfected glioblastoma cell line (U373-GFP). After U373-GFP cells were settled into microwells and chemically lysed, electromigration of GFP was monitored during single-cell PAGE via epifluorescence microscopy. We calibrated local GFP electrophoretic mobility in the pore-gradient gel to mobilities measured in uniform pore-size chemically polymerized gels (4%T, 6%T, 8%T, 10%T, 12%T, 16%T,

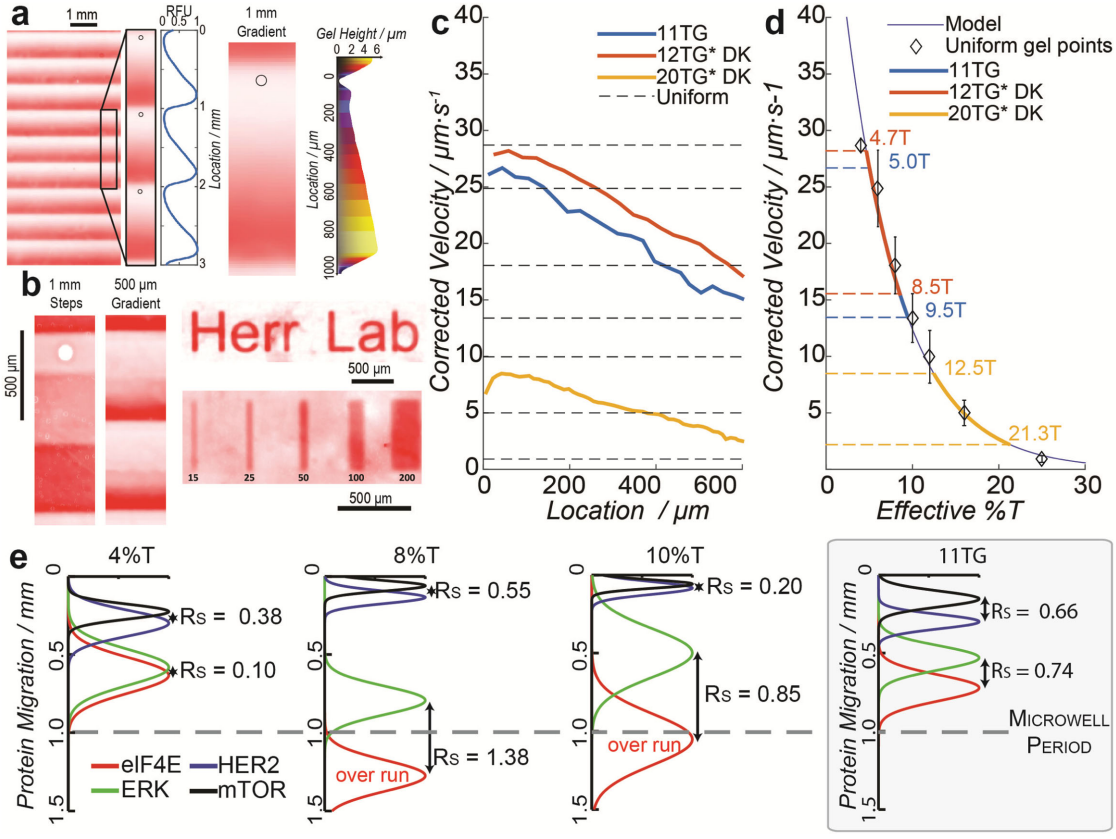

Figure 2. Grayscale photomask patterning creates a dense array of pore-gradient gels capable of resolving HER2-related signaling proteins within each 1 mm long PAGE separation lane. a) Fluorescence micrograph of a pore-gradient microgel incorporating allylamine for FITC visualization of gel density.[26] Optical profilometry shows gel height increase along the pore-size gradient. b) Fluorescence micrographs show patterned gel density. c) Viscosity-corrected GFP velocities decrease along the large-to-small pore gradient, with average viscosity-corrected velocities from uniform gels plotted as dotted horizontal lines. Analysis performed on single U373-GFP cells. d) Calibration curve[28] relates local effective gel density in pore-gradient gels, spanning from 5%T-to-9.5%T for 11TG (red), 4.7%T-to-8.5%T for 12TG*DK (blue), and 12.5%T-to-21.3%T for 20TG*DK (yellow). n = 3–5 independent experiments, with standard deviations shown. e) Averaged Gaussian fits of fluorescence intensity for SKBR3 single-cell protein separations under three uniform gel density conditions (4, 8, and 10%T) and an 11TG pore-gradient gel. Four target proteins involved in HER2 signaling are assayed: eIF4E (25 kDa; red), ERK (44 kDa; green), HER2 (185 kDa; blue), and mTOR (289 kDa; black), with the separation resolution (R_s) noted for protein pairs at the extremes of the molecular mass range (HER2-mTOR and eIF4E-ERK). Protein peaks that overrun the 1 mm separation length are noted. n = 3 independent experiments, E = 40 V cm^{-1}, cell lysis time is 20 s for U373-GFP cells and 25 s for SKBR3 cells.

and 25%T, $n = 3$, where %T is the total amount of acrylamide; Figure 2c,d).

From theory, we anticipate electrophoresis along a linear pore-gradient gel (low-to-high gel density) to yield nonlinear distance–time relationships, with protein velocity inversely related to time and exponentially related to gel density. In practice, we observed an increase in GFP electrophoretic mobility with time in the uniform gels, which was not expected (Figure S5, Supporting Information). In this system, Joule heating raises the local temperature, lowering the local viscosity and, thus, increasing the apparent electrophoretic mobility of all proteins. To account for these Joule heating related effects in uniform pore-size gels, we relate the observed velocity (U_{ob}) and initial velocity (U_0) to electrophoresis time, t, by $U_{ob} = U_0 e^{0.026*b*t}$ where $b = 0.81 \pm 0.11$ [°C s^{-1}] and the constant 0.026 is the expected decrease in viscosity per degree Celsius.[27] To decouple temperature-induced effects from the sieving effects, we then solve for the viscosity-corrected velocity, $U_{corr} = U_{ob} e^{-0.026*b*t}$ (Figure S6, Supporting Information). As expected, the viscosity correction results in a nearly constant GFP velocity in uniform pore-size gels, thus allowing study of sieving along each pore-gradient microgel. Nonlinear GFP electrophoretic mobilities in various pore-gradient microgels were observed (Figure 2c). Using Ferguson's relationship between local electrophoretic mobility and apparent gel density for GFP,[28] we can design optimal grayscale photopatterning conditions to optimize separation resolution for the targets of interest (Figure 2d).

A key application for the pore-gradient microgel array is to study the protein signaling at single-cell resolution, particularly important in cancer. Signaling dysregulation and heterogeneity underlie patient outcomes.[29,30] Human epidermal growth factor receptor 2 (HER2, a.k.a. ERBB2) positive breast cancer (BCa) accounts for 25% of breast cancers.[31] Overexpression of HER2 triggers multiple downstream protein activations, and cross-talk between pathways makes HER2-positive BCa aggressive with low survival rate.[32,33] Here we assay HER2-related signaling proteins in individual breast tumor cells. The signaling proteins include: eIF4E (25 kDa), ERK (44 kDa), HER2 (185 kDa), and mTOR (289 kDa), spanning a molecular mass range that encompasses ~80% of the mammalian proteome (estimated using NIH3T3 cells).[34] We use an 11%T PAG precursor to create pore-gradient microgels with effective gel density ranging from 5%T to 9.5%T (abbreviated as 11TG to denote gradient gel). We first performed single-cell western blotting on single HER2-positive breast cancer cells (SKBR3), with separation performance in pore-gradient microgels (11TG) compared to that in uniform pore-size gels (4%T, 8%T, and 10%T; Figure 2e and Figure S7, Supporting Information). The fitted Gaussian curves in Figure 2e are used to identify the relative location of each protein peak.

To evaluate molecular sieving by ascertaining resolution of neighboring peaks, the separation resolution (R_s) is calculated from peak-to-peak displacement normalized by average peak width[35] with $R_s \geq 0.5$ defined as an acceptable separation resolution. Gaussian fitting identifies peak center and peak width when an $R^2 > 0.7$ goodness of fit threshold is surpassed. Additionally, the protein electrophoretic mobilities (μ) are calculated for each protein across a range of different gel densities (Table S2, Supporting Information). While large uniform pore-size gels (4%T) resolved the high molecular mass protein pair (HER2-mTOR), the small molecular mass protein pair (eIF4E-ERK) was not resolvable ($R_s = 0.38 \pm 0.5$ for mTOR-HER2, $n = 327$; and $R_s = 0.1 \pm 0.02$ for eIF4E-ERK, $n = 230$; at 40 V cm^{-1} for 8 s). Uniform, moderate pore-size gels (8%T) resolved both high and low molecular mass protein pairs, but reduced the array density as 50% longer separation distance was required to resolve the small mass proteins ($R_s = 0.55 \pm 0.31$ for HER2-mTOR, $n = 1446$; and $R_s = 1.38 \pm 0.31$ for eIF4E-ERK, $n = 1498$; at 40 V cm^{-1} for 25 s). Uniform, small pore-size gels (10%T) resolved the low molecular mass protein pair, but the high molecular mass protein pair could not electromigrate into the sieving gel from the microwell ($R_s = 0.85 \pm 0.16$ for eIF4E-ERK, $n = 2252$; at 40 V cm^{-1} for 30 s). So while uniform gels successfully resolved similarly sized proteins, resolving pairs at both ends of the molecular mass range was a challenge in the required short separation lengths. In contrast, in the 1 mm long pore-gradient microgels (5%T–9.5%T) all three protein pairs exceeded the critical R_s ($R_s > 0.65$ for mTOR-HER2, HER2-ERK, and ERK-eIF4E) in 15 s of elapsed separation time (at 40 V cm^{-1}). Thus, pore-gradient microgels enhanced separation resolution for protein pairs across the wide 25-to-289 kDa range in the 1 mm separation distances needed for the microwell array format.

Next, in the pore-expansion prong of our study, we designed a gel to decouple the local pore-size requirements in the PAGE stage of the single-cell western blot from requirements posed by in-gel immunoprobing. To do this, we created a large-to-small pore-size gradient gel that can be switched to a uniform, large pore-size immobilization scaffold for spatially unbiased in-gel immunoprobing. In addition, the polymer is designed to be compatible with buffers used in all stages of the single-cell western blot (cell settling, electrophoresis, photoblotting, and antibody probing). We selected this chemistry, as acid-labile ketal cross-linkers have been employed to enhance recovery of intact proteins and nucleic acids with gel solubilization after electrophoresis.[36,37] Further, the cross-linker is especially well suited to our single-cell western blot, as the ketal group is stable in neutral-to-basic buffers,[38] and rapid hydrolysis at low pH yields an inert gel product.[39]

To achieve pore expansion, we introduced a dual cross-linker system, Figure 1d, employing both BIS and DK cross-linker chemistries. In the DK cross-linker, acid hydrolysis of the ketal group expanded gel pores facilitating diffusion of antibody into the gel during immunoprobing. The stable BIS cross-linker maintained the physical integrity of the gel structure, as is critical to retaining the immobilized proteins and separation information. Other cross-linker formulations have been reported for gel pore expansion including partial gel de-cross-linking of *N,N*-Bisacryloyl-1,2-dihydroxy-1,2-ethylenediamine using periodic acid treatment to create large pore-size gels[40]—but the reaction induces protein modifications that may impact immunoreactivity. Base-labile ethylene glycol diacrylate has also been useful for peptide recovery after electrophoresis in mass spectroscopy,[41] but is unstable in the neutral-to-basic buffers required in single-cell western blotting and forms a charged product.

To characterize immunoprobing in BIS and DK gel, we again used GFP as a protein target and defined probing efficiency as $\eta = AUC_{probed}/AUC_{GFP}$ where area-under-the-curve (AUC) is calculated from each single-cell western blot protein peak. We first

Adv. Mater. 2015,
DOI: 10.1002/adma.201503939

established baseline η values, by measuring immunoprobing of GFP from the U373-GFP model system in chemically polymerized uniform pore-size gels containing no DK (6%T, 8%T, 10%T, and 12%T; **Figure 3**a). In these uniform, fully cross-linked gels, we observed a nearly three orders of magnitude decrease in η in the smallest pore-size gel, as compared to the largest pore-size gel (12%T versus 6%T). Partitioning of proteins and antibodies out of hydrogels increases exponentially with gel density.[42]

To characterize η along a 1 mm long pore-gradient microgel, we immunoprobed GFP from U373-GFP cells subjected to a range of single-cell electrophoresis times (10, 15, 20, and 30 s). The electrophoresis times locate the GFP peaks at different positions along the separation axis and, hence, in different local gel densities (Figure 3b). In a 5%T-to-9.5%T gradient gel (11TG), we observed an order-of-magnitude decrease in η along the 1 mm separation axis (Figure 3c,d; $\eta_{5\%T} = 13.62 \pm 7.89$, $n = 318$; $\eta_{9.5\%T} = 1.36 \pm 1.76$, $n = 71$). As we had hypothesized, the bias in η along the separation axis severely limits quantification of protein targets in non-de-cross-linked pore-gradient microgels.

To evaluate η after pore expansion, we substituted the DK cross-linker for 99% of BIS in the gel precursor solution on a mol per mol basis[43] (Table S1, Supporting Information). The optimized dual cross-linker PAG formulation consists of 11.28% (w/v) acrylamide, 0.0072% (w/v) BIS, and 1.247% (w/v) DK. We fabricated 1 mm long dual cross-linked pore-gradient microgels with an effective gel density ranging from 4.7%T to 8.5%T (abbreviated as 12TG*DK). After PAGE and protein immobilization we aggressively de-cross-linked the gel using a 1% HCl solution (pH 1.1) with rheometry suggesting de-cross-linking in the first 10 min of the reaction. We adopted a conservative 30 min de-cross-linking period with detailed kinetics in Figure S9 (Supporting Information). After de-cross-linking and to remove any residual acid, gels were equilibrated in Tris-buffered saline with Tween 20 (TBST) for ≈30 min prior to probing. We observe $\eta_{4.7\%T} = 2.69 \pm 1.24$ ($n = 188$) at the head of the pore-gradient microgel (low density region) and $\eta_{8.5\%T} = 2.33 \pm 0.97$ ($n = 123$) at the terminus of the microgel (high density region) (Figure 3c,e). While we observed reduced η in the large pore-size

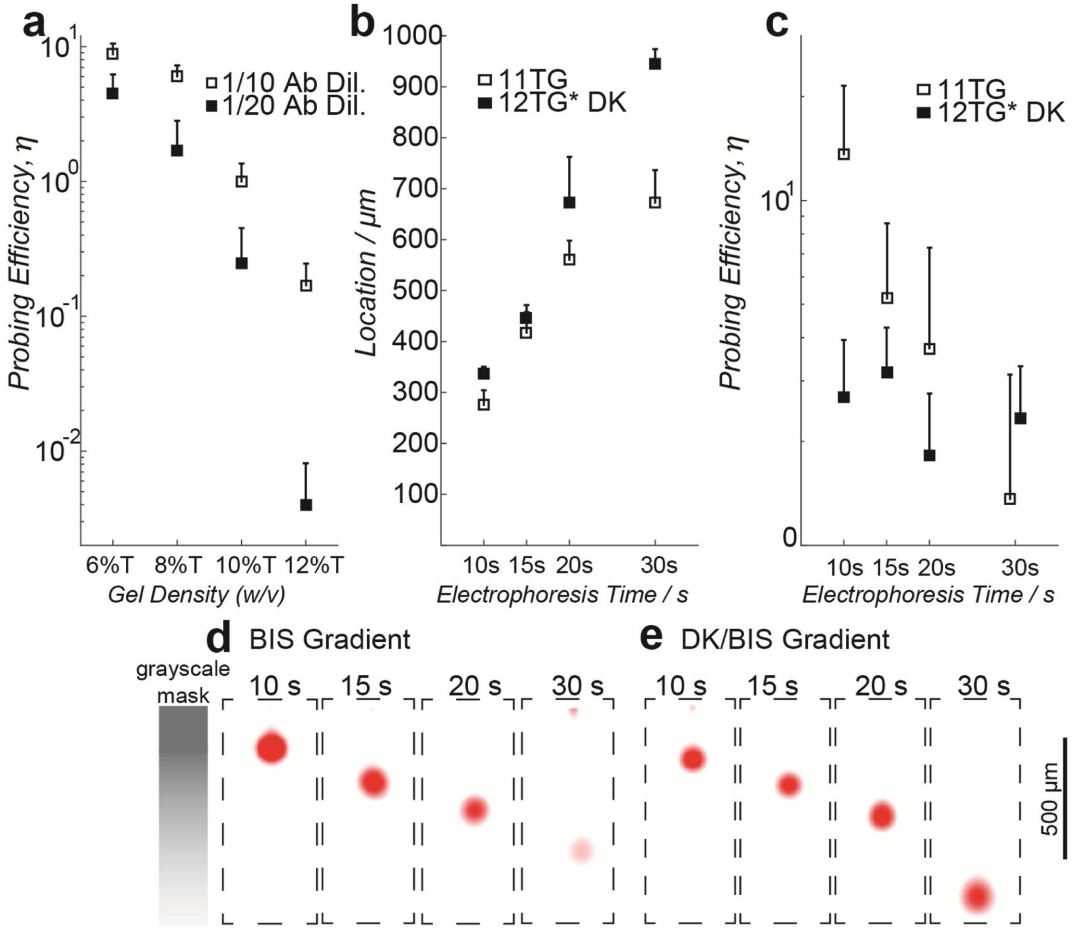

Figure 3. Cleavage of cross-linker mitigates nonuniform antibody probing along the pore-gradient gel separation axis. a) Probing efficiency in uniform density gels is inversely related to gel density. The probing efficiency of single, lysed U373-GFP cells is calculated by normalizing the immunoprobed GFP signal to native GFP signal. b) Location of probed GFP peak is a function of electrophoresis duration in BIS and DK cross-linked gels. GFP peak location and, hence, local gel density allow assessment of nonuniform probing efficiency along the separation axis. c) Probing efficiency along pore-gradient gels is nearly independent of local gel density after hydrogel de-cross-linking. d,e) Fluorescence micrographs of probed GFP peaks in BIS pore-gradient gels and de-cross-linked DK/BIS pore-gradient gels. $n = 3$–5 independent experiments, half standard deviation shown, $E = 40$ V cm^{-1}, cell lysis time is 20 s.

region of the de-cross-linked gels compared to the BIS gels, we observed an enhanced η in the small pore-size region of the gel. Thus, the pore-size modulation nearly eliminated location-dependent probing bias along the separation axis, regardless of the initial pore-size of the sieving matrix. Further application of dual cross-linked pore-gradient microgels (12TG*DK) on SKBR3 breast cancer cells showed similar performance in DK (Figure 1a, right panel) comparing to BIS gradient gel (Figure 2e and Figure S7, Supporting Information).

Finally, we applied pore-gradient microgels to study HER2-related signaling in single cells dissociated from a human HER2-positive breast tumor biopsy (**Figure 4**a and Section S11, Supporting Information). We adjusted the lysis buffer for primary human cells (1% sodium dodecyl sulfate (SDS), 1% sodium deoxycholate, and 0.1% Triton at 50 °C for 25 s) from the formulation used for the SKBR3 cell line. Using a 5%T-to-9.5%T pore-gradient microgel array (11TG), we resolved both the largest and mid-range protein pairs (R_s = 0.53 ± 0.19, n = 9 for mTOR-HER2 and R_s = 1.15 ± 0.5, n = 23 for HER2-ERK, at 40 V cm^{-1} for 15 s) with R_s comparable to that observed in SKBR3 experiments (Figure 2e and Figure S7, Supporting Information). In the primary tumor cells, we observed stronger signal from high molecular mass species and larger eIF4E peak dispersion. Observed peak dispersion suggests a sensitive dependence on cell type, including substantial differences in the lysis behavior of cell lines as compared to primary tumor cells. In cell lines versus primary cells, differences in eIF4E peak dispersion may arise from the formation of eIF4E translation–initiation complexes in the primary tumor cells[44] or to the insolubility of the eIF4E protein complex in tumor cells.[14] Intriguingly, we observe a 50-fold difference (maximum-to-minimum ratio) in HER2 expression among the primary breast tissue cells (coefficient of variation, CV = 0.74, n = 37; Figure 4b,c, with protein quantification and data analysis in the Section S8, Supporting Information). Clinically, IHC is the principal protein-based diagnostic tool for HER2-positive status. Although widely used, IHC provides only qualitative and subjective readouts. In the case of the HER2 protein, IHC reports strong (+++), intermediate (++), weak (+), and negative (0) staining in >10% tumor cells in an area of tumor.[45] In contrast, the single-cell western blot verifies the HER2 status (33/37, ≈90% of HER2-positive cells), while also

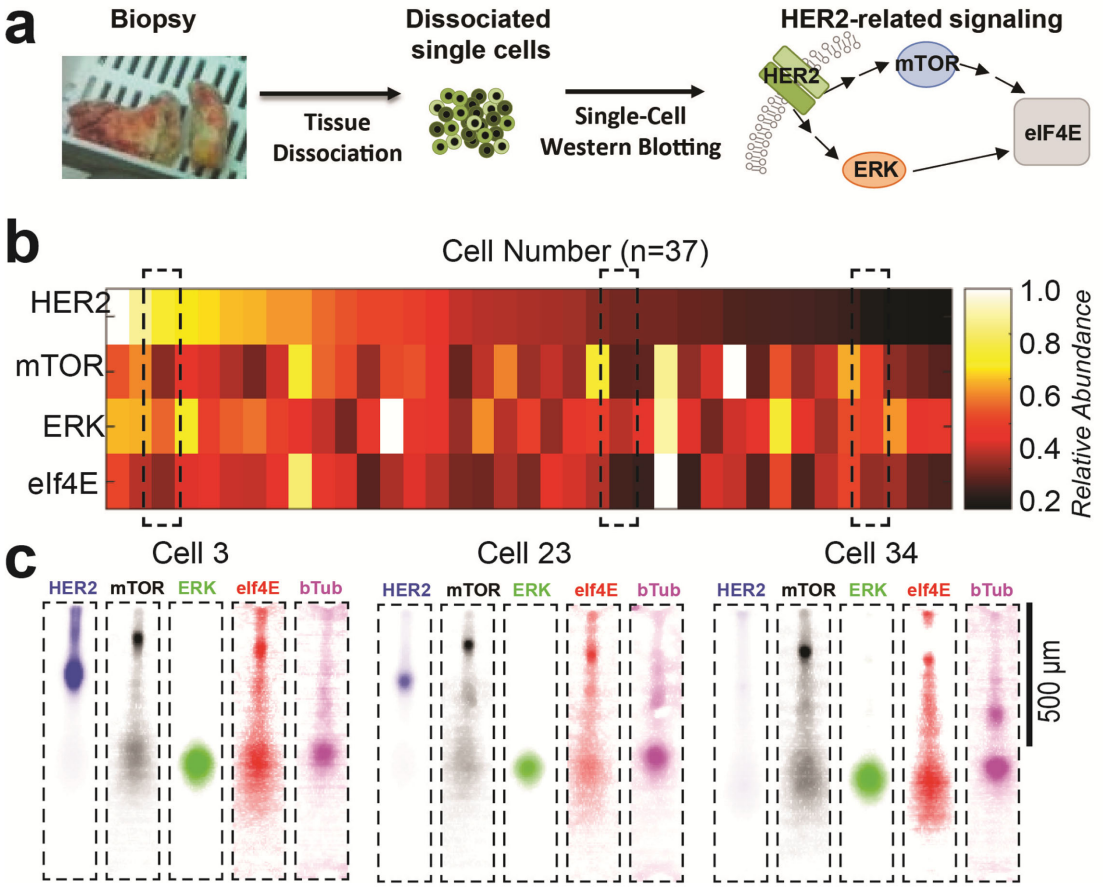

Figure 4. Pore-gradient western blots of single, dissociated primary HER2-positive breast tumor cells. a) A HER2-positive breast cancer biopsy is dissociated into single tumor cells for assessing the intratumoral heterogeneity in the HER2-related protein signaling. b) Relative expression levels of four HER2-relevant proteins (HER2, mTOR, ERK, and eIF4E) in single human tumor cells. Protein expression is normalized to β-tubulin in each cell and then normalized to the strongest signal for each target across the entire cell population. c) Fluorescence micrographs of selected single-cell western blots show high, medium, and low HER2 expression, heterogeneous mTOR, ERK, and eIF4E expression, and similar β-tubulin expression levels. E = 40 V cm^{-1}, cell lysis time is 25 s.

Adv. Mater. **2015**,
DOI: 10.1002/adma.201503939

reporting semi-quantitative levels of expression. While intratumoral HER2 heterogeneity is an independent prognostic factor for disease-free survival,[46] multiple downstream signaling pathways dictate drug resistance to targeted HER2 therapy.[47] The mTOR,[48] ERK,[32] and eIF4E[44] proteins are related to both independent and cross-talk mechanisms of trastuzumab resistance, making assessment of a panel of proteins important to defining the intratumoral variation. Among these primary tumor cells, five to tenfold differences in mTOR, ERK, and eIF4E expression were observed (Figure S10, Supporting Information). Inclusion of phospho-specific antibodies would indicate activation state of the signaling proteins.

To conclude, we detail advances in single-cell protein separation science using spatial and temporal control of PAG, a material that is a cornerstone of separation science. Using two compatible photoresponsive chemistries, thousands of 1 mm long pore-gradient microgels (each aligned with a microwell) are created on a standard microscope slide. Grayscale photopatterning spatially modulates the PAG polymerization kinetics and, hence, local pore-size. Photopatterning is designed for compatibility with benzophenone methacrylamide cross-linked into the polymer to allow for post-electrophoresis protein immobilization (blotting). Pore-gradient microgels resolve a wide mass range of proteins which is essential for assessing signaling pathways implicated in cancer progression. Further, we incorporate acid-labile DK cross-linkers in the polymer for pore expansion after blotting to support unbiased in-gel immunoprobing. Overall, separation-based-targeted proteomics with single-cell resolution endows researchers with a powerful tool for in-depth high-throughput studies on signaling pathways and cell-to-cell variation. More broadly, this new analytical technology links single-cell response to the protein expression, modifications, and interactions that drive cellular phenotype, such as tumor progression and drug resistance.

Experimental Section

Dual Cross-Linked Pore-Gradient PAG Fabrication: For the optimized dual cross-linked pore-gradient PAG (12TG*DK), 99/1 molar ratio of cross-linkers (0.06%C(w/w) of 40% (w/v) 29:1 acrylamide/bis-acrylamide (Sigma, A7802) and 9.95%C(w/w) of DK (synthesized in house, Supporting Information Section S7)) in the precursor solution with 1% (w/v) VA-086 (photoinitiator, Waco Chemical), 3 mM benzophenone methacrylamide (PharmAgra Laboratories), and acrylamide monomer (40% (w/v) acrylamide solution, Sigma, A4058) was prepared for photopolymerization. The grayscale of the mask was designed in the plotting program CleWin4 using a simple algorithm in a MATLAB script (Supporting Information Section S3). The mask was further fabricated on soda lime glass by aBeam Technologies (Hayward, CA, USA), which was able to fabricate masks with tens of millions of features (necessary in grayscale patterns). The glass-SU8 mold was fabricated through a general photolithography process (Supporting Information Section S10). Before UV-activated photopolymerization, the glass-SU8 mold and the grayscale chrome mask were aligned under an inverted microscope with 1 gradient period abutting each lane of microwells (Figure 1b and Figure S1, Supporting Information). After carefully moving the assembled fabrication setup onto the UV illumination system (OAI, San Jose, CA, USA), the setup in the order of the light path was: UV filter, grayscale chrome mask, glass-SU8 mold, gel precursor solution, and a methacrylate-functionalized glass slide (Figure S1, Supporting Information). In one UV exposure, the dual cross-linked pore-gradient gel can be fabricated.

Single-Cell Pore-Gradient Western Blotting and Pore Expansion: Primary HER2-positive tissue was procured from Stanford Tissue Bank under both Stanford and Berkeley Institutional Review Board (IRB) permission. The handling of single-cell western blotting on BIS and DK gradient gel, including single-cell settling, in situ lysis, PAGE, photoactivated protein immobilization, immunoblotting, and imaging, was similar to that on the uniform gel.[13,14] The DK gel was de-cross-linked after protein immobilization to facilitate pore expansion for subsequent immunoblotting. The details are given in the Section S2 and S11, Supporting Information.

Supporting Information

Supporting Information is available from the Wiley Online Library or from the author.

Acknowledgements

T.A.D. and C.-C.K. contributed equally to this work. T.A.D., C.-C.K., and A.E.H. designed the wide molecular mass single-cell western blot assay. T.A.D., C.-C.K., and A.E.H. designed experiments. T.A.D. designed software and performed analysis for fluorescence quantitation, separation resolution, and multiplexing. Data were analyzed by T.A.D. and C.-C.K. S.M. synthesized the DK molecule. All authors wrote the manuscript. T.A.D., C.-C.K., and A.E.H. are inventors on pending patents related to single-cell protein analysis methods. A.E.H. holds equity interest in commercialization efforts. The authors thank Dr. Jessica Bockhorn in the Pegram Lab for assisting with tumor tissue dissociation; and the QB3 Biomolecular Nanotechnology Center (BNC) at UC Berkeley for partial infrastructure support. T.A.D. is a National Science Foundation Graduate Research Fellow. This work was partially supported by a U.S. National Institutes of Health (NIH) New Innovator Award (DP2OD007294 to A.E.H.), a National Science Foundation CAREER award (CBET-1056035 to A.E.H.), an NIH Innovative Molecular Analysis Technology award (CA183679 to A.E.H.), and a UC Berkeley Bakar Fellowship (to A.E.H), as well as a Susan G. Komen Investigator Initiated Award (IIR12222976 to M.D.P.).

Received: August 12, 2015
Revised: October 5, 2015
Published online:

[1] D. Hanahan, R. A. Weinberg, *Cell* **2011**, *144*, 646.
[2] B. N. Rexer, C. L. Arteaga, *Cancer Res.* **2013**, *73*, 3817.
[3] A. M. Scott, J. P. Allison, J. D. Wolchok, *Cancer Immun.* **2012**, *12*, 14.
[4] E. C. Stack, C. Wang, K. A. Roman, C. C. Hoyt, *Methods* **2014**, *70*, 46.
[5] S. P. Perfetto, P. K. Chattopadhyay, M. Roederer, *Nat. Rev. Immunol.* **2004**, *4*, 648.
[6] D. R. Bandura, V. I. Baranov, O. I. Ornatsky, A. Antonov, R. Kinach, X. Lou, S. Pavlov, S. Vorobiev, J. E. Dick, S. D. Tanner, *Anal. Chem.* **2009**, *81*, 6813.
[7] J. S. Mellors, K. Jorabchi, L. M. Smith, J. M. Ramsey, *Anal. Chem.* **2010**, *82*, 967.
[8] C. Stadler, E. Rexhepaj, V. R. Singan, R. F. Murphy, R. Pepperkok, M. Uhlen, J. C. Simpson, E. Lundberg, *Nat. Methods* **2013**, *10*, 315.
[9] H. T. Maecker, J. Trotter, *Cytometry Part A* **2006**, *69A*, 1037.
[10] W. N. Burnette, *Anal. Biochem.* **1981**, *112*, 195.
[11] S. Jin, G. J. Anderson, R. T. Kennedy, *Anal. Chem.* **2013**, *85*, 6073.
[12] A. J. Hughes, A. E. Herr, *Proc. Natl. Acad. Sci. USA* **2012**, *109*, 21450.
[13] A. J. Hughes, D. P. Spelke, Z. Xu, C. C. Kang, D. V. Schaffer, A. E. Herr, *Nat. Methods* **2014**, *11*, 749.
[14] C. C. Kang, J. M. Lin, Z. Xu, S. Kumar, A. E. Herr, *Anal. Chem.* **2014**, *86*, 10429.

[15] S. Mura, J. Nicolas, P. Couvreur, *Nat. Mater.* **2013**, *12*, 991.
[16] H. Z. An, M. E. Helgeson, P. S. Doyle, *Adv. Mater.* **2012**, *24*, 3838.
[17] O. Chaudhuri, S. T. Koshy, C. Branco da Cunha, J. W. Shin, C. S. Verbeke, K. H. Allison, D. J. Mooney, *Nat. Mater.* **2014**, *13*, 970.
[18] D. W. Hutmacher, *Nat. Mater.* **2010**, *9*, 90.
[19] M. P. Lutolf, G. P. Raeber, A. H. Zisch, N. Tirelli, J. A. Hubbell, *Adv. Mater.* **2003**, *15*, 888.
[20] D. Rodbard, G. Kapadia, A. Chrambach, *Anal. Biochem.* **1971**, *40*, 135.
[21] J. Margolis, K. G. Kenrick, *Nature* **1967**, *214*, 1334.
[22] R. C. Ebersole, R. P. Foss (E.I. DU PONT De Nemours and Company), U.S. 4,704,198, **1987**.
[23] J. E. Poelma, B. P. Fors, G. F. Meyers, J. W. Kramer, C. J. Hawker, *Angew. Chem. Int. Ed.* **2013**, *125*, 6982.
[24] S. Park, D. Kim, S. Y. Ko, J. O. Park, S. Akella, B. Xu, Y. Zhang, S. Fraden, *Lab Chip* **2014**, *14*, 1551.
[25] J. Y. Wong, A. Velasco, P. Rajagopalan, Q. Pham, *Langmuir* **2003**, *19*, 1908.
[26] A. Buxboim, K. Rajagopal, B. Andre'EX, D. E. Discher, *J. Phys.: Condens. Mater* **2010**, *22*, 194116.
[27] J. H. Knox, I. H. Grant, *Chromatographia* **1987**, *24*, 135.
[28] K. A. Ferguson, *Metabolism* **1964**, *13*, 985.
[29] V. Almendro, A. Marusyk, K. Polyak, *Annu. Rev. Pathol.* **2013**, *8*, 277.
[30] R. Fisher, L. Pusztai, C. Swanton, *Br. J. Cancer* **2013**, *108*, 479.
[31] D. J. Slamon, G. M. Clark, S. G. Wong, W. J. Levin, A. Ullrich, W. L. McGuire, *Science* **1987**, *235*, 177.
[32] V. Serra, M. Scaltriti, L. Prudkin, P. J. Eichhorn, Y. H. Ibrahim, S. Chandarlapaty, B. Markman, O. Rodriguez, M. Guzman, S. Rodriguez, M. Gili, M. Russillo, J. L. Parra, S. Singh, J. Arribas, N. Rosen, J. Baselga, *Oncogene* **2011**, *30*, 2547.
[33] D. Zardavas, J. Baselga, M. Piccart, *Nat. Rev. Clin. Oncol.* **2013**, *10*, 191.
[34] J. J. Li, P. J. Bickel, M. D. Biggin, *Peer J.* **2014**, *2*, e270.
[35] J. C. Giddings, *Unified Separation Science*, Wiley, NY **1991**.
[36] Y. K. Kim, Y. J. Kwon, *Proteomics* **2009**, *9*, 3765.
[37] Y. K. Kim, Y. J. Kwon, *Electrophoresis* **2010**, *31*, 1656.
[38] R. Jain, S. M. Standley, J. M. J. Fréchet, *Macromolecules* **2007**, *40*, 452.
[39] Y. J. Kwon, S. M. Standley, A. P. Goodwin, E. R. Gillies, J. M. J. Fréchet, *Mol. Pharm.* **2005**, *2*, 83.
[40] P. Arenkov, A. Kukhtin, A. Gemmell, S. Voloshchuk, V. Chupeeva, A. Mirzabekov, *Anal. Biochem.* **2000**, *278*, 123.
[41] S. Bornemann, B. Rietschel, S. Baltruschat, M. Karas, B. Meyer, *Electrophoresis* **2010**, *31*, 585.
[42] J. Tong, J. L. Anderson, *Biophys. J.* **1996**, *70*, 1505.
[43] P. G. Righetti, B. C. W. Brost, R. S. Snyder, *J. Biochem. Biophys. Methods* **1981**, *4*, 347.
[44] P. Zindy, Y. Berge, B. Allal, T. Filleron, S. Pierredon, A. Cammas, S. Beck, L. Mhamdi, L. Fan, G. Favre, J. P. Delord, H. Roche, F. Dalenc, M. Lacroix-Triki, S. Vagner, *Cancer Res.* **2011**, *71*, 4068.
[45] A. C. Wolff, M. E. Hammond, D. G. Hicks, M. Dowsett, L. M. McShane, K. H. Allison, D. C. Allred, J. M. Bartlett, M. Bilous, P. Fitzgibbons, W. Hanna, R. B. Jenkins, P. B. Mangu, S. Paik, E. A. Perez, M. F. Press, P. A. Spears, G. H. Vance, G. Viale, D. F. Hayes, *J. Clin. Oncol.* **2013**, *31*, 3997.
[46] H. Seol, H. J. Lee, Y. Choi, H. E. Lee, Y. J. Kim, J. H. Kim, E. Kang, S. W. Kim, S. Y. Park, *Mod. Pathol.* **2012**, *25*, 938.
[47] A. T. Baker, A. Zlobin, C. Osipo, *Front. Oncol.* **2014**, *4*, 360.
[48] S. Vinayak, R. W. Carlson, *Oncology* **2013**, *27*, 38.

Adv. Mater. **2015**,
DOI: 10.1002/adma.201503939